Chromatic Aberration Correction for Atomic Resolution TEM Imaging from 20 to 80 kV

Martin Linck,* Peter Hartel, Stephan Uhlemann, Frank Kahl, Heiko Müller, Joachim Zach, and Max. Haider
Corrected Electron Optical Systems GmbH, Englerstrasse 28, D-69126 Heidelberg, Germany

Marcel Niestadt and Maarten Bischoff
FEI Company, Achtseweg Noord 5, 5651 GG Eindhoven, Netherlands

Johannes Biskupek, Zhongbo Lee, Tibor Lehnert, Felix Börrnert, Harald Rose, and Ute Kaiser
Central facility of electron microscopy, Ulm University, Albert-Einstein-Allee 11, D-89081 Ulm, Germany
(Received 22 April 2016; published 9 August 2016)

Atomic resolution in transmission electron microscopy of thin and light-atom materials requires a rigorous reduction of the beam energy to reduce knockon damage. However, at the same time, the chromatic aberration deteriorates the resolution of the TEM image dramatically. Within the framework of the SALVE project, we introduce a newly developed C_c/C_s corrector that is capable of correcting both the chromatic and the spherical aberration in the range of accelerating voltages from 20 to 80 kV. The corrector allows correcting axial aberrations up to fifth order as well as the dominating off-axial aberrations. Over the entire voltage range, optimum phase-contrast imaging conditions for weak signals from light atoms can be adjusted for an optical aperture of at least 55 mrad. The information transfer within this aperture is no longer limited by chromatic aberrations. We demonstrate the performance of the microscope using the examples of 30 kV phase-contrast TEM images of graphene and molybdenum disulfide, showing unprecedented contrast and resolution that matches image calculations.

DOI: 10.1103/PhysRevLett.117.076101

Since the dawn of aberration-corrector technology, transmission electron microscopy (TEM) has routinely provided insights into the structure of matter with true atomic resolution for accelerating voltages from 80 to 300 kV [1–4]. Unfortunately, specimens consisting of light elements like carbon materials, oxides, and lithium compounds can suffer severe damage via the knockon mechanism [5–8]. Consequently, imaging at lower acceleration voltages, from 60 to 80 kV, became widespread in order to undercut the threshold for knockon damage. Thanks to C_s correction, an image resolution of about 0.2 nm can be maintained even for these low voltages [9–11]. However, the main interest when performing atomic resolution microscopy on these thin and light element materials lies in interfaces and defects. For such structures, the knockon damage threshold is significantly lower, demanding even smaller electron energies [12]. However, at the same time ionization damage—known as radiolysis—also increases. Therefore, the final choice of electron energy depends on each individual sample's compromise between ionization and knockon damage [13]. Fortunately, there are possibilities to reduce radiolysis effects via sample preparation [14,15].

The resolving power of a fixed-beam transmission electron microscope is determined by the geometrical and chromatic aberrations of the imaging system and the stability of the instrumental setup [12,16]. At low acceleration voltages, the information limit in the phase-contrast image is dominated by the chromatic focus spread. Therefore, low-voltage TEM requires either very special imaging techniques (such as tilt-series reconstruction [17], optimized ultrahigh resolution lenses, and cold FEG emitters [18]) or monochromation of the primary electrons [19]. However, these measures do not prevent inelastically scattered electrons from being strongly defocused at the image plane. This can only be avoided by correction of the chromatic aberration.

As an alternative approach, the SALVE project [20] has been initiated to develop a dedicated low-voltage TEM that is corrected for both the spherical and the chromatic aberration, allowing for true atomic-resolution TEM observations on beam-sensitive materials with an accelerating voltage from only 20 to 80 kV. For this purpose a standard TEM column was equipped with a special low-voltage quadrupole-octupole-type C_c/C_s corrector.

In this Letter we characterize the achieved information limit and the optical transfer function for different high tensions. We measure the higher-rank residual chromatic aberrations and the remaining parasitic focus spread. Finally, we present atomically resolved images of single-layer graphene and molybdenum disulfide (MoS_2) taken at 30 kV.

Figure 1 demonstrates the direct benefits of C_c/C_s correction at 20 kV by comparing images of small gold clusters on thin carbon film taken with an uncorrected TEM, a C_s-only corrected TEM [$C_c = 1.45$ mm, $\sigma(E) \approx 0.35$ eV], and the SALVE instrument. In uncorrected TEMs, chromatic and spherical aberrations severely limit the resolution. Therefore, the information content in Fourier space is limited to a small optical aperture.

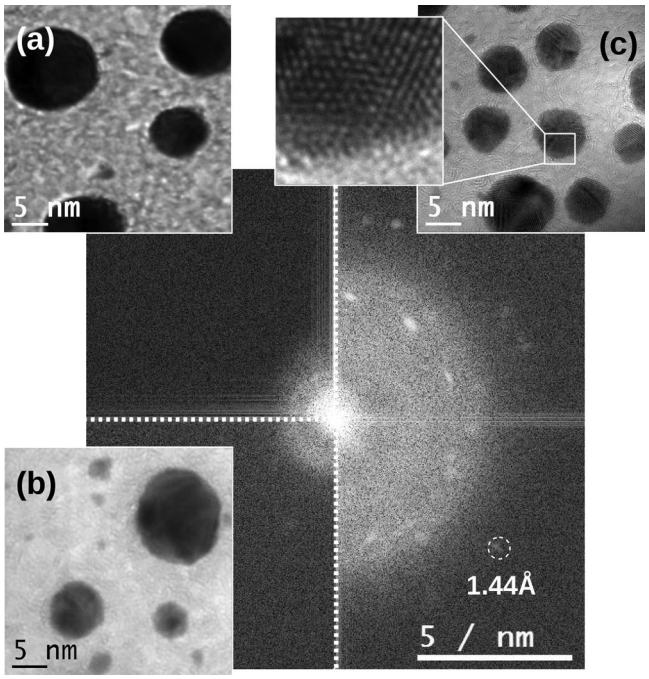

FIG. 1. TEM images of small gold clusters on thin carbon film at 20 kV with diffractograms obtained in (a) an uncorrected TEM, (b) a C_s-only corrected TEM and (c) the C_c/C_s-corrected SALVE TEM. Only panel (c) shows the Au clusters atomically resolved.

Although the delocalization vanishes in the C_s-corrected TEM, the resolution hardly improves. In an image recorded with our C_c/C_s-corrected TEM, Fourier space is filled with specimen information up to very large aperture angles; information is transferred down to the size of individual atoms. The Au [022] reflections corresponding to a lattice spacing of 144 pm are clearly visible in the diffractogram.

The centerpiece of the SALVE microscope is a novel C_c/C_s corrector based on the so-called Rose-Kuhn design [21]. This quadrupole-octupole corrector consists of eight multipole stages. Of those magnetic dodecapole elements, two are capable of simultaneously producing electrostatic quadrupole fields. The correction of the chromatic aberration is achieved by a superposition of electrostatic and magnetostatic quadrupole fields, whereas the spherical aberration is compensated by a certain combination of magnetostatic octupole fields [22]. At the top, two transfer lenses are used to adapt the corrector to the objective lens; at the bottom, two adapter lenses couple the corrector to the projective system. Figure 2 shows a photograph of the corrector and a schematic ray path. The corrector has 104 channels in total, which—if controlled properly—allow for correcting axial aberrations up to and including fifth order and off-axial aberrations up to and including third order. The intrinsic fifth-order spherical aberration C_5 can be adjusted by design to positive values from 2 to 5 mm. This provides optimum conditions for bright-atom phase contrast [23] and allows atomic-resolution imaging with large fields of view. The corrector is incorporated into a FEI Titan Themis^3 microscope equipped with a standard SuperTwin

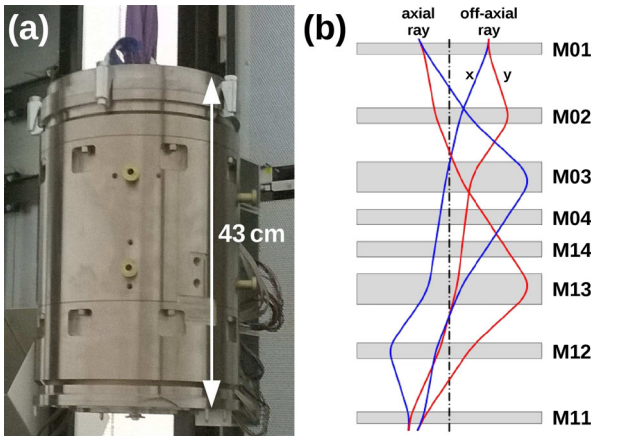

FIG. 2. (a) Photograph of the SALVE C_c/C_s corrector during installation into the TEM column. It adds 43 cm of length and about 185 kg of weight to the TEM column. (b) The corrector consists of eight multipoles. Here, the axial and off-axial rays in the x section (blue) and the y section (red) are overlaid to the corrector scheme.

objective lens and a high-brightness Schottky-type electron source (FEI X-FEG).

The TEM's information limit is affected by three fundamental parameters: the spatial coherence of the illumination, the focus spread in the imaging optics, and the image spread resulting from Johnson noise [24]. The information-dampening effect due to partial spatial coherence could be reduced dramatically by the correction of the spherical aberration [1]. Thereafter, the focus spread due to the chromatic aberration of the objective lens remained the main limitation for low-voltage TEM imaging [12]. The energy-dependent defocus $C_1(\triangle E) = -\sum_i C_{1c}^{(i)} k^i$ expanded to a power series with respect to the chromatic parameter $k = \triangle E/E$ with nominal beam energy E is strictly dominated by the linear coefficient $C_c = C_{1c}^{(1)}$ for any uncorrected TEM. The higher-degree coefficients only have to be taken into account in C_c-corrected instruments [25]. The chromatic aberration translates the energy spread of the electron source and instabilities of the accelerating voltage into a focus spread. After C_c correction, an additional focus spread—caused by instabilities of the focusing elements due to noise from the electronics' supplies—remains. Therefore, all lens and quadrupole currents, as well as correction voltages, have to be extremely stable [16]. In addition, thermally driven magnetic field noise (Johnson noise) had to be considered. The stochastic beam deflections that are generated by every conductor (both magnetic and nonmagnetic) result in a resolution-limiting image spread that strongly depends on the electrons' ray path and the shape of the metal parts close to the beam [24]. A trade-off between the bore of the multipole elements, the lens gaps, and the liner tube diameter was made that enabled the required correction strength and focusing power and, at the same time, prevented the electron beam from suffering too much image spread. This succeeded at the edge of technological

TABLE I. Resulting information limit and its aperture equivalent for the SALVE microscope at different accelerating voltages compared to the 50 mrad lattice spacing.

High voltage	Wavelength	50 mrad spacing	Experimental information limit	Aperture equivalent
20 kV	8.589 pm	171.8 pm	139 pm	62 mrad
30 kV	6.979 pm	139.6 pm	115 pm	61 mrad
40 kV	6.016 pm	120.3 pm	90 pm	67 mrad
60 kV	4.866 pm	97.3 pm	83 pm	59 mrad
80 kV	4.176 pm	83.5 pm	76 pm	55 mrad

feasibility in that, for example, the magnetic materials in the multipoles were exploited close to magnetic saturation.

Table I summarizes the achieved TEM information transfer of the C_c/C_s-corrected SALVE microscope and Fig. 3 shows the corresponding results of the Young's fringe resolution test on an amorphous tungsten sample of 2 nm thickness recorded on a Gatan US1000XP CCD camera. The Supplemental Material provides an alternative assessment of information transfer to confirm the Young's fringe results [26–29]. For all aligned high tensions, the determined resolution values exceed the specification of an effective 50 mrad imaging aperture.

For proper use of the complete transferred information, the wave aberration function has to be controlled accurately in this angular range. The round aberrations, i.e., defocus C_1 and spherical aberrations of third-order C_3 and fifth-order C_5, require tuning to specific values to establish a uniform PCTF beyond the 50 mrad aperture. All noncircular aberrations that disturb uniform phase contrast have to be corrected as much as possible [30]. The measured 20 kV phase plate in Fig. 3(f) indicates that this challenging task has been accomplished with the SALVE corrector. Moreover, off-axial aberrations including off-axial coma have also been tuned sufficiently small to provide a considerable field of view with a stable aberration function.

For the well-aligned state in the SALVE microscope, the different contributions to focus spread have been characterized. The linear chromatic aberration is compensated and achromaticity is only violated by higher-rank chromatic aberrations. Figure 4(a) compares the energy-dependent defocus at 20 kV of a C_c-uncorrected TEM ($C_{1c}^{(1)} = C_c = 1.45$ mm) and the SALVE microscope. The C_c-uncorrected case shows a very steep linear gradient, whereas the SALVE measurements follow a third-order polynomial fit with the first- to third-degree chromatic coefficients $C_c = C_{1c}^{(1)} = 1.176\ \mu\text{m} \approx 0$, $C_{1c}^{(2)} = 6.621$ mm, and $C_{1c}^{(3)} = 148.2\text{mm}$. These values roughly meet the theoretical predictions from optical models. The magnified area in Fig. 4(a) illustrates the capabilities for EFTEM at 20 kV: within an energy window of 20 eV the defocus changes by only ~2 nm compared to 1.45 μm for the C_c-uncorrected setup. This advantage is expected to enable new modes of operation, such as high-resolution EFTEM [31], at very low accelerating voltages.

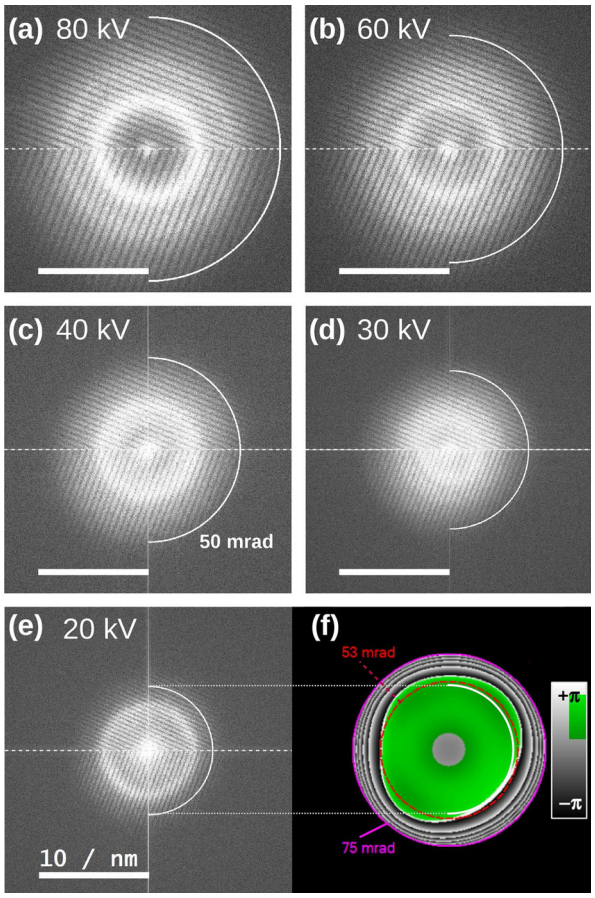

FIG. 3. The microscope's resolution at (a) 80 kV, (b) 60 kV (c) 40 kV (d) 30 kV, and (e) 20 kV as determined by Young's fringes on an amorphous tungsten sample. The FFTs of the images are equally scaled (10 nm^{-1} scale bar) and show the results for two perpendicular directions (upper and lower half, respectively), indicating uniform information transfer exceeding 50 mrad (white half circle) for all accelerating voltages. (f) The measured aberration function χ of the 20 kV setting shows that a uniform phase contrast transfer function (PCTF) can be tuned in the SALVE corrector [phase plate χ to scale with (e); green color illustrates where $\sin\chi > 0.5$]. The corresponding aberration coefficients are listed in the Supplemental Material [26].

The parasitic focus spread $\sigma(C_1)$ caused by the limited stability of the focusing elements has been estimated by comparing the information transfer under axial and tilted illumination. In the case of a tilted illumination, the focus spread in an uncorrected microscope would dramatically reduce the information transfer in the tilt direction [25]. In the SALVE microscope, however, as seen in Fig. 4(b), even a beam tilt of 3° (52.4 mrad) does not affect the information transfer noticeably. As a consequence, it is very difficult to quantify the focus spread in detail; we can only give an upper limit of $\sigma(C_1) \leq 1$ nm at 20 kV. This value represents the statistic deviation of the information limit in terms of a focus spread as evaluated from series of images. Evidently, this value is negligible compared to the focus spread of $\sigma(C_1) \approx 25$ nm for a nonmonochromated, C_c-uncorrected microscope at 20 kV [$C_c = 1.45$ mm,

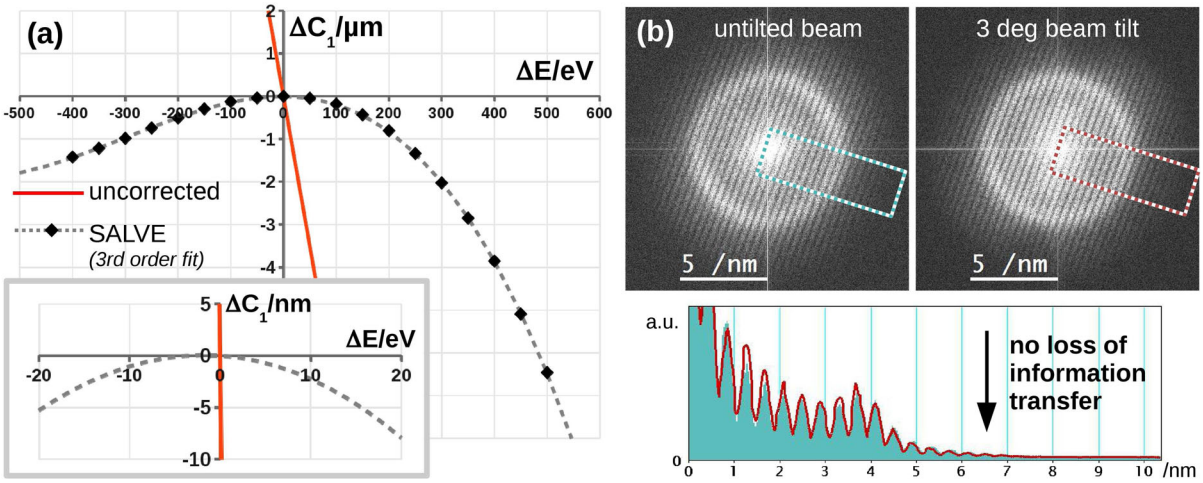

FIG. 4. (a) Achromaticity at 20 kV: In C_c-uncorrected TEMs (red line: $C_c = 1.45$ mm) the defocus changes dramatically with a change of electron energy. In the SALVE microscope (black dots: measurement; dashed line: third-order fit) the energy-dependent defocus changes only due to the remaining quadratic and cubic chromatic aberrations. (b) Estimation of focus spread: The information transfer under axial illumination (solid profile) does not show any deterioration at all if the beam is tilted to 3° (52.4 mrad) (red line in profile).

$\sigma(E) \approx 0.35$ eV]. This experiment proves that the corrector's supplies satisfy the very strict requirements for C_c correction. To achieve the same focus spread in such a C_c-uncorrected TEM by means of a monochromator, the energy width of the gun would have to be limited to $\sigma(E) \approx 14$ meV even without taking into account the instabilities of accelerating voltage and objective lens current. For this case, an ideal monochromator would cut out about 96% of the available beam current. Moreover, independent from monochromation, inelastically scattered electrons would still be defocused very strongly by the chromatic aberration of the objective lens.

Figure 5 shows, as demonstration examples, images of freestanding monolayers of graphene and MoS_2 at an accelerating voltage of 30 kV. In the raw experimental images (1 s exposure time, 2048×2048 frame size) the accumulated electron doses are $2.5 \times 10^6\ e^-/\mathrm{nm}^2$ and $3 \times 10^5\ e^-/\mathrm{nm}^2$ for graphene and MoS_2, respectively. The diffractogram of graphene reveals reflections up to third order, corresponding to 107 pm. For MoS_2, even the fourth-order reflections, i.e., 102 pm, can be detected in the diffractogram. Although the raw data are very noisy, it is possible to identify the single carbon atoms in the hexagonal lattice under those dose-limited conditions. Moreover, molybdenum can clearly be distinguished from the two sulfur atoms, which are located underneath each other in this crystal projection. The signal-to-noise ratio caused by the limited electron dose can be enhanced by postprocessing as described in the Supplemental Material [26]. The averaged images of graphene and MoS_2 show a strongly improved single-atom contrast and are in good agreement with the simulated images. The demonstrated resolution within the HRTEM images obtained at 30 kV and the achieved match between experimental and

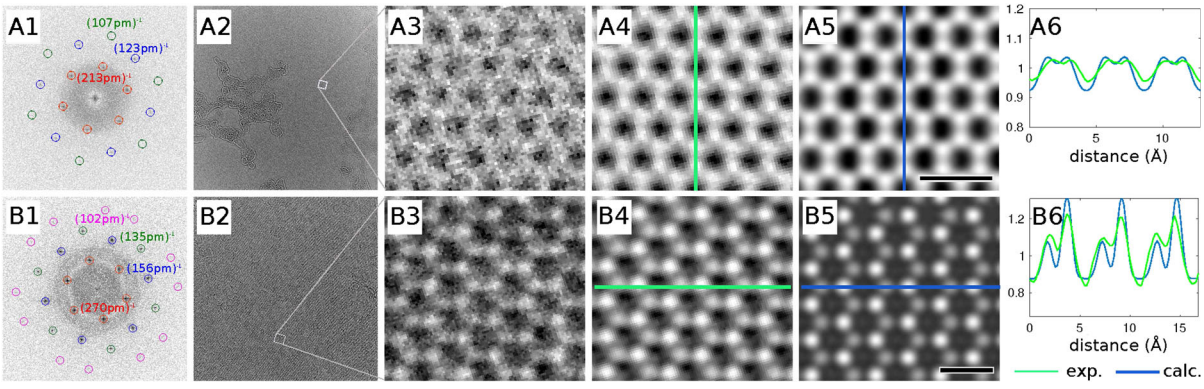

FIG. 5. Experimental and calculated C_c/C_s-corrected 30-kV HRTEM images of graphene (A) and MoS_2 (B). The diffractograms (A1 and B1) of the experimental raw images of graphene (A2) and MoS_2 (B2) in bright-atom contrast (field of view 40×40 nm^2) indicate the achieved resolution. The magnified images (A3 and B3) directly allow for identifying the atomic structure. The averaged experimental images (A4 and B4) show a strong signal-to-noise improvement and are in good agreement with the simulated images (A5 and B5) as visible in the corresponding line profiles (A6 and B6). The scale bars in A5 and B5 correspond to 0.5 nm.

calculated image contrast—if further developed to a truly quantitative match—will not only allow for detecting single atoms and point-defect structures but also for determining their chemical nature. In the movie in the Supplemental Material [32], we show that an edge configuration in graphene that is reproducibly unstable at 80 kV [33,34] hardly changes when imaged at only 30 kV.

We successfully demonstrated the functionality of a TEM corrector for geometric and chromatic aberration correction for voltages from 20 to 80 kV. Between 40 and 80 kV, even subangstrom resolution has been shown. The demonstrated information limit of 90 pm at 40 kV corresponds to a maximum aperture angle of 67 mrad. This is a new record in phase-contrast TEM imaging: The achieved resolution corresponds to only 15 times the electron wavelength. Furthermore, the correction of chromatic aberration opens up new opportunities for analytic imaging because large energy windows are almost equally well focused at the image plane.

The examples of graphene and MoS_2 demonstrate that the stability and resolution of the complete system (microscope and corrector) is more than sufficient to resolve single atoms in raw TEM images at 30 kV. At the current lowest-possible voltage of 20 kV, a resolution better than 0.14 nm can be achieved allowing even for atomic or near-atomic imaging. This is a huge step forward towards materials analysis on delicate, beam-sensitive objects; the SALVE microscope now combines both the desired resolution and the beam energy below knockon threshold at the same time.

The authors acknowledge funding from the German Research Foundation (DFG) and the Ministry of Science, Research and the Arts (MWK) of the federal state of Baden-Württemberg, Germany. Dr. Roger A. Wepf (ETH Zürich, CH) is acknowledged for providing us with the amorphous tungsten sample.

*linck@ceos-gmbh.de

[1] M. Haider, S. Uhlemann, E. Schwan, H. Rose, B. Kabius, and K. Urban, Nature (London) **392**, 768 (1998).
[2] C. Kisielowski, B. Freitag, M. Bischoff, H. Van Lin, S. Lazar, G. Knippels, P. Tiemeijer, M. van der Stam, S. von Harrach, M. Stekelenburg *et al.*, Microsc. Microanal. **14**, 469 (2008).
[3] K. W. Urban, Science **321**, 506 (2008).
[4] Z. Zhang and U. Kaiser, Ultramicroscopy **109**, 1114 (2009).
[5] F. Banhart, Rep. Prog. Phys. **62**, 1181 (1999).
[6] R. Egerton, P. Li, and M. Malac, Micron **35**, 399 (2004).
[7] J. C. Meyer, F. Eder, S. Kurasch, V. Skakalova, J. Kotakoski, H. J. Park, S. Roth, A. Chuvilin, S. Eyhusen, G. Benner *et al.*, Phys. Rev. Lett. **108**, 196102 (2012).
[8] F. Wang, J. Graetz, M. S. Moreno, C. Ma, L. Wu, V. Volkov, and Y. Zhu, ACS Nano **5**, 1190 (2011).
[9] O. L. Krivanek, M. F. Chisholm, V. Nicolosi, T. J. Pennycook, G. J. Corbin, N. Dellby, M. F. Murfitt, Z. S. Szilagyi, M. P. Oxley, S. T. Pantelides *et al.*, Nature (London) **464**, 571 (2010).
[10] K. Suenaga and M. Koshino, Nature (London) **468**, 1088 (2010).
[11] N. Alem, O. V. Yazyev, C. Kisielowski, P. Denes, U. Dahmen, P. Hartel, M. Haider, M. Bischoff, B. Jiang, S. G. Louie *et al.*, Phys. Rev. Lett. **106**, 126102 (2011).
[12] U. Kaiser, J. Biskupek, J. Meyer, J. Leschner, L. Lechner, H. Rose, M. Stöger-Pollach, A. Khlobystov, P. Hartel, H. Müller *et al.*, Ultramicroscopy **111**, 1239 (2011).
[13] R. Egerton, Ultramicroscopy **145**, 85 (2014).
[14] G. Algara-Siller, S. Kurasch, M. Sedighi, O. Lehtinen, and U. Kaiser, Appl. Phys. Lett. **103**, 203107 (2013).
[15] T. W. Chamberlain, J. Biskupek, S. T. Skowron, P. A. Bayliss, E. Bichoutskaia, U. Kaiser, and A. N. Khlobystov, Small **11**, 510 (2015).
[16] M. Haider, H. Müller, S. Uhlemann, J. Zach, U. Loebau, and R. Hoeschen, Ultramicroscopy **108**, 167 (2008).
[17] A. Kirkland, W. Saxton, K.-L. Chau, K. Tsuno, and M. Kawasaki, Ultramicroscopy **57**, 355 (1995).
[18] T. Sasaki, H. Sawada, F. Hosokawa, Y. Sato, and K. Suenaga, Ultramicroscopy **145**, 50 (2014).
[19] S. Morishita, M. Mukai, K. Suenaga, and H. Sawada, Appl. Phys. Lett. **108**, 013107 (2016).
[20] U. A. Kaiser, *Project homepage of the Sub-Angstrom Low Voltage Electron Microscopy and Spectroscopy (SALVE) project* (Ulm University, Germany, 2016), http://www.salve-project.de/.
[21] H. Rose, in *Electron Microscopy 92: Proceedings of the 10th European Congress on Electron Microscopy, Granada, Spain, 7–11 September 1992* (Secretariado de Publicaciones de la Universidad de Granada, Granada, 1992).
[22] O. Scherzer, Optik (Munich, Ger.) **2**, 114 (1947).
[23] C.-L. Jia, M. Lentzen, and K. Urban, Microsc. Microanal. **10**, 174 (2004).
[24] S. Uhlemann, H. Müller, P. Hartel, J. Zach, and M. Haider, Phys. Rev. Lett. **111**, 046101 (2013).
[25] M. Haider, P. Hartel, H. Müller, S. Uhlemann, and J. Zach, Microsc. Microanal. **16**, 393 (2010).
[26] See Supplemental Material at http://link.aps.org/supplemental/10.1103/PhysRevLett.117.076101, which includes Refs. [24,25,27–29], for aberration coefficients, an alternative resolution assessment, image processing details and a description of the supplemental movie.
[27] H. Müller, I. Maßmann, S. Uhlemann, P. Hartel, J. Zach, and M. Haider, Nucl. Instrum. Methods Phys. Res., Sect. A **645**, 20 (2011).
[28] J. Barthel and A. Thust, Phys. Rev. Lett. **101**, 200801 (2008).
[29] K. Kimoto, K. Kurashima, T. Nagai, M. Ohwada, and K. Ishizuka, Ultramicroscopy **121**, 31 (2012).
[30] P. Hartel, M. Linck, F. Kahl, H. Müller, and M. Haider, Microsc. Microanal. **20**, 926 (2014).
[31] K. W. Urban, J. Mayer, J. R. Jinschek, M. J. Neish, N. R. Lugg, and L. J. Allen, Phys. Rev. Lett. **110**, 185507 (2013).
[32] See Supplemental Material at http://link.aps.org/supplemental/10.1103/PhysRevLett.117.076101 for the supplemental movie.
[33] J. Kotakoski, D. Santos-Cottin, and A. V. Krasheninnikov, ACS Nano **6**, 671 (2012).
[34] K. Suenaga, Y. Iizumi, and T. Okazaki, Eur. Phys. J. Appl. Phys. **54**, 33508 (2011).